

Partial Wave Analysis of $\chi_{c0} \rightarrow \pi^+\pi^-K^+K^-$

M. Ablikim¹, J. Z. Bai¹, Y. Ban¹¹, J. G. Bian¹, X. Cai¹, H. F. Chen¹⁶, H. S. Chen¹, H. X. Chen¹, J. C. Chen¹, Jin Chen¹, Y. B. Chen¹, S. P. Chi², Y. P. Chu¹, X. Z. Cui¹, Y. S. Dai¹⁸, Z. Y. Deng¹, L. Y. Dong^{1a}, Q. F. Dong¹⁴, S. X. Du¹, Z. Z. Du¹, J. Fang¹, S. S. Fang², C. D. Fu¹, C. S. Gao¹, Y. N. Gao¹⁴, S. D. Gu¹, Y. T. Gu⁴, Y. N. Guo¹, Y. Q. Guo¹, Z. J. Guo¹⁵, F. A. Harris¹⁵, K. L. He¹, M. He¹², Y. K. Heng¹, H. M. Hu¹, T. Hu¹, G. S. Huang^{1b}, X. P. Huang¹, X. T. Huang¹², X. B. Ji¹, X. S. Jiang¹, J. B. Jiao¹², D. P. Jin¹, S. Jin¹, Yi Jin¹, Y. F. Lai¹, G. Li², H. B. Li¹, H. H. Li¹, J. Li¹, R. Y. Li¹, S. M. Li¹, W. D. Li¹, W. G. Li¹, X. L. Li⁸, X. Q. Li¹⁰, Y. L. Li⁴, Y. F. Liang¹³, H. B. Liao⁶, C. X. Liu¹, F. Liu⁶, Fang Liu¹⁶, H. H. Liu¹, H. M. Liu¹, J. Liu¹¹, J. B. Liu¹, J. P. Liu¹⁷, R. G. Liu¹, Z. A. Liu¹, F. Lu¹, G. R. Lu⁵, H. J. Lu¹⁶, J. G. Lu¹, C. L. Luo⁹, F. C. Ma⁸, H. L. Ma¹, L. L. Ma¹, Q. M. Ma¹, X. B. Ma⁵, Z. P. Mao¹, X. H. Mo¹, J. Nie¹, S. L. Olsen¹⁵, H. P. Peng¹⁶, N. D. Qi¹, H. Qin⁹, J. F. Qiu¹, Z. Y. Ren¹, G. Rong¹, L. Y. Shan¹, L. Shang¹, D. L. Shen¹, X. Y. Shen¹, H. Y. Sheng¹, F. Shi¹, X. Shi^{11c}, H. S. Sun¹, J. F. Sun¹, S. S. Sun¹, Y. Z. Sun¹, Z. J. Sun¹, Z. Q. Tan⁴, X. Tang¹, Y. R. Tian¹⁴, G. L. Tong¹, G. S. Varner¹⁵, D. Y. Wang¹, L. Wang¹, L. S. Wang¹, M. Wang¹, P. Wang¹, P. L. Wang¹, W. F. Wang^{1d}, Y. F. Wang¹, Z. Wang¹, Z. Y. Wang¹, Zhe Wang¹, Zheng Wang², C. L. Wei¹, D. H. Wei¹, N. Wu¹, X. M. Xia¹, X. X. Xie¹, B. Xin^{8b}, G. F. Xu¹, Y. Xu¹⁰, M. L. Yan¹⁶, F. Yang¹⁰, H. X. Yang¹, J. Yang¹⁶, Y. X. Yang³, M. H. Ye², Y. X. Ye¹⁶, Z. Y. Yi¹, G. W. Yu¹, C. Z. Yuan¹, J. M. Yuan¹, Y. Yuan¹, S. L. Zang¹, Y. Zeng⁷, Yu Zeng¹, B. X. Zhang¹, B. Y. Zhang¹, C. C. Zhang¹, D. H. Zhang¹, H. Y. Zhang¹, J. W. Zhang¹, J. Y. Zhang¹, Q. J. Zhang¹, X. M. Zhang¹, X. Y. Zhang¹², Yiyun Zhang¹³, Z. P. Zhang¹⁶, Z. Q. Zhang⁵, D. X. Zhao¹, J. W. Zhao¹, M. G. Zhao¹⁰, P. P. Zhao¹, W. R. Zhao¹, Z. G. Zhao^{1e}, H. Q. Zheng¹¹, J. P. Zheng¹, Z. P. Zheng¹, L. Zhou¹, N. F. Zhou¹, K. J. Zhu¹, Q. M. Zhu¹, Y. C. Zhu¹, Y. S. Zhu¹, Yingchun Zhu^{1f}, Z. A. Zhu¹, B. A. Zhuang¹, X. A. Zhuang¹, B. S. Zou¹.

(BES Collaboration)

¹ *Institute of High Energy Physics, Beijing 100049, People's Republic of China*

² *China Center of Advanced Science and Technology, Beijing 100080, People's Republic of China*

³ *Guangxi Normal University, Guilin 541004, People's Republic of China*

⁴ *Guangxi University, Nanning 530004, People's Republic of China*

⁵ *Henan Normal University, Xinxiang 453002, People's Republic of China*

⁶ *Huazhong Normal University, Wuhan 430079, People's Republic of China*

⁷ *Hunan University, Changsha 410082, People's Republic of China*

⁸ *Liaoning University, Shenyang 110036, People's Republic of China*

⁹ *Nanjing Normal University, Nanjing 210097, People's Republic of China*

¹⁰ *Nankai University, Tianjin 300071, People's Republic of China*

¹¹ *Peking University, Beijing 100871, People's Republic of China*

¹² *Shandong University, Jinan 250100, People's Republic of China*

¹³ *Sichuan University, Chengdu 610064, People's Republic of China*

¹⁴ *Tsinghua University, Beijing 100084, People's Republic of China*

¹⁵ *University of Hawaii, Honolulu, HI 96822, USA*

¹⁶ *University of Science and Technology of China, Hefei 230026, People's Republic of China*

¹⁷ *Wuhan University, Wuhan 430072, People's Republic of China*

¹⁸ *Zhejiang University, Hangzhou 310028, People's Republic of China*

^a *Current address: Iowa State University, Ames, IA 50011-3160, USA*

^b *Current address: Purdue University, West Lafayette, IN 47907, USA*

^c *Current address: Cornell University, Ithaca, NY 14853, USA*

^d *Current address: Laboratoire de l'Accélérateur Linéaire, F-91898 Orsay, France*

^e *Current address: University of Michigan, Ann Arbor, MI 48109, USA*

^f *Current address: DESY, D-22607, Hamburg, Germany*

A partial wave analysis of $\chi_{c0} \rightarrow \pi^+\pi^-K^+K^-$ in $\psi(2S) \rightarrow \gamma\chi_{c0}$ decay is presented using a sample of 14 million $\psi(2S)$ events accumulated by the BES II detector. The data are fitted to the sum of relativistic covariant tensor amplitudes for intermediate resonant decay modes. From the fit, significant contributions to χ_{c0} decays from the channels $f_0(980)f_0(980)$, $f_0(980)f_0(2200)$, $f_0(1370)f_0(1710)$, $K^*(892)^0\bar{K}^*(892)^0$, $K_0^*(1430)\bar{K}_0^*(1430)$, $K_0^*(1430)\bar{K}_2^*(1430) + c.c.$, and $K_1(1270)K$ are found. Flavor-SU(3)-violating $K_1(1270) - K_1(1400)$ asymmetry is observed. Values obtained for the masses and widths of the resonances $f_0(1710)$, $f_0(2200)$, $f_0(1370)$, and $K_0^*(1430)$ are presented.

PACS numbers: 13.25.Gv, 12.38.Qk, 14.40.Gx

I. INTRODUCTION

Exclusive heavy quarkonium decays constitute an important laboratory for investigating perturbative QCD. Compared to J/ψ decays, relatively little is known concerning χ_{cJ} ($J = 0, 1, 2$) decays [1]. More experimental data on exclusive decays of P-wave charmonia are important for a better understanding of the nature of χ_{cJ} states, as well as testing QCD based calculations. Further, the decays of χ_{cJ} , in particular χ_{c0} and χ_{c2} , provide a direct window on glueball dynamics in the 0^{++} and 2^{++} channels, as the χ_{cJ} hadronic decays may proceed via $c\bar{c} \rightarrow gg \rightarrow q\bar{q}q\bar{q}$ [2].

Amplitude analysis of χ_{cJ} decays is an excellent tool for studying charmonium decay dynamics. Knowledge of the quantum mechanical decay amplitude allows one to investigate not only the intermediate resonant decay modes but also to properly account for the interference effects between different resonances.

In this paper, partial wave analysis results of $\chi_{c0} \rightarrow \pi^+\pi^-K^+K^-$ in $\psi(2S) \rightarrow \gamma\chi_{c0}$ decays using 14 million $\psi(2S)$ events accumulated at the BESII detector are presented. In previous studies of this channel, only the decay modes $\chi_{c0} \rightarrow K^+\bar{K}^*(892)^0\pi^- + c.c.$ and $K^*(892)^0\bar{K}^*(892)^0$ were measured [3, 4]. Here additional information from partial wave analysis is very important.

II. BES DETECTOR

BESII is a large solid-angle magnetic spectrometer that is described in detail in Ref. [5]. Charged particle momenta are determined with a resolution of $\sigma_p/p = 1.78\%\sqrt{1+p^2}$ (p in GeV/ c) in a 40-layer cylindrical drift chamber. Particle identification (PID) is accomplished by specific ionization (dE/dx) measurements in the drift chamber and time-of-flight (TOF) measurements in a barrel-like array of 48 scintillation counters. The dE/dx resolution is $\sigma_{dE/dx} = 8.0\%$; the TOF resolution is $\sigma_{TOF} = 180$ ps for Bhabha events. Outside of the TOF system is a 12 radiation length lead-gas barrel shower counter (BSC), operating in self-quenching streamer mode, that measures the positions and energies of electrons and photons over 80% of the total solid angle. The energy resolution is $\sigma_E/E = 22\%/\sqrt{E}$ (E in GeV). Surrounding the BSC is a solenoid magnet that provides a 0.4 T magnetic field in the central tracking region of the detector. Three double-layer muon counters instrument the magnet flux return and serve to identify muons with momentum greater than 0.5 GeV/ c . They cover 68% of the total solid angle.

In this analysis, a GEANT3 based Monte Carlo (MC) simulation package (SIMBES) with detailed consideration of detector performance (such as dead electronic channels) is used. The consistency between data and MC has been checked in many high purity physics channels, and the agreement is quite reasonable [6].

III. EVENT SELECTION

The selection criteria described below are similar to those used in previous BES analyses [4, 7].

A. Photon identification

A neutral cluster is considered to be a photon candidate when the angle between the nearest charged track and the cluster is greater than 15° , the first hit is in the beginning six radiation lengths, and the difference between the angle of the cluster development direction in the BSC and the photon emission direction is less than 30° . The photon candidate with the largest energy deposit in the BSC is treated as the photon radiated from the $\psi(2S)$ and used in a four-constraint (4-C) kinematic fit to the hypothesis $\psi(2S) \rightarrow \gamma\pi^+\pi^-K^+K^-$.

B. Charged particle identification

Each charged track, reconstructed using MDC information, is required to be well fit to a three-dimensional helix, be in the polar angle region $|\cos\theta_{MDC}| < 0.80$, and have the point of closest approach of the track to the beam axis be within 2 cm of the beam axis and within 20 cm from the center of the interaction region along the beam line. For each track, the TOF and dE/dx measurements are used to calculate χ^2 values and the corresponding confidence levels for the hypotheses that the particle is a pion, kaon, or proton.

C. Event selection criteria

Candidate events are required to satisfy the following selection criteria:

- (1) The number of charged tracks is required to be four with net charge zero.
- (2) The sum of the momenta of the two lowest momentum tracks with opposite charges is required to be greater than 650 MeV/c; this removes contamination from $\psi(2S) \rightarrow \pi^+\pi^-J/\psi$ events.
- (3) The confidence level for the 4-C kinematic fit to the decay hypothesis $\psi(2S) \rightarrow \gamma\pi^+\pi^-K^+K^-$ is required to be greater than 0.01.

The combined confidence level determined from the 4-C kinematic fit and PID information is used to separate $\gamma\pi^+\pi^-\pi^+\pi^-$, $\gamma K^+K^-K^+K^-$, and the different possible particle assignments for the $\gamma\pi^+\pi^-K^+K^-$ final states. This combined confidence level is defined as

$$\int_{\chi_{all}^2}^{\infty} f(z; ndf_{all}) dz,$$

where $f(z; ndf_{all})$ is the χ^2 probability density function, χ_{all}^2 is the sum of the χ^2 values from the 4-C kinematic fit and those of the four track PID assignments, and ndf_{all} is the corresponding total number of degrees of freedom. For an event to be selected, the combined confidence level of $\gamma\pi^+\pi^-K^+K^-$ must be larger than those of the other possibilities. In addition, the PID confidence level of each charged track must be > 0.01 .

Further rejection against $K_S^0 \rightarrow \pi^+\pi^-$ is obtained by requiring that any $\pi^+\pi^-K^+K^-$ combination with $M_{\pi^+\pi^-}$ in the interval (497 ± 50) MeV/c² should have $r_{xy} < 5$ mm, where r_{xy} is the distance from the beam axis to the $\pi^+\pi^-$ vertex.

The invariant mass distribution for the $\pi^+\pi^-K^+K^-$ events that survive all the above selection requirements is shown in Fig. 1. There are clear peaks corresponding to the χ_{cJ} states. The highest mass peak corresponds to $\psi(2S)$ decays to four charged track final states that are kinematically fitted with an unassociated, low energy photon.

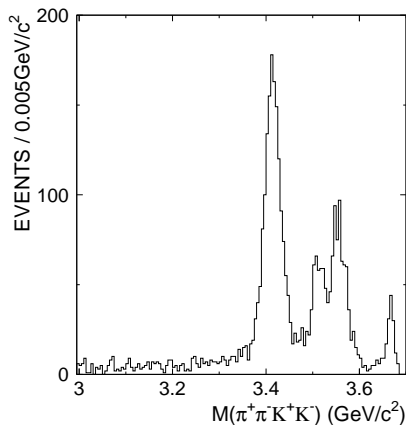


FIG. 1: The $\pi^+\pi^-K^+K^-$ invariant mass spectrum. There are three clear χ_{cJ} peaks. The highest mass peak corresponds to $\psi(2S)$ decays to four charged tracks final states that are kinematically fitted with an unassociated, low energy photon.

An additional five-constraint (5-C) kinematic fit is made with the invariant mass of the $\pi^+\pi^-K^+K^-$ being constrained to the χ_{c0} mass. After requiring the confidence level for the 5-C fit to be greater than 0.01, the $\pi^+\pi^-K^+K^-$ invariant mass distributions for data and MC, shown in Fig. 2, are obtained, where the $\pi^+\pi^-K^+K^-$ invariant mass obtained from the 4-C fit and the generated mass and width of the χ_{c0} are fixed to PDG values [1]. The agreement found in this comparison indicates a clean data sample suitable for partial wave analysis in which the four-momentum information from the 5-C fit will be used. Finally, 1371 $\psi(2S) \rightarrow \gamma\chi_{c0}$, $\chi_{c0} \rightarrow \pi^+\pi^-K^+K^-$ candidate events are selected after all the above criteria.

Figure 3 shows the individual K^+K^- , $\pi^+\pi^-$, $K\pi$, $K\pi\pi$, and $KK\pi$ invariant mass distributions. There are two strong symmetric structures at about 1.75 GeV/c² and 2.2 GeV/c² and some evidence for $f_0(980)$ in the K^+K^- mass distribution, and there are clear $\rho(770)$ and $f_0(980)$ peaks and a smaller one at about 1.3 GeV/c² in the $\pi^+\pi^-$ mass distribution. There is no obvious structure for the $KK\pi$ mass spectrum in Fig. 3.

Fig. 4(a) shows the scatter plot of K^+K^- versus $\pi^+\pi^-$ invariant mass for selected $\psi(2S) \rightarrow \gamma\chi_{c0}$, $\chi_{c0} \rightarrow \pi^+\pi^-K^+K^-$ events, which provides further information on the intermediate resonant decay modes for $(\pi^+\pi^-)(K^+K^-)$ decay. For instance, it can be seen that the $f_0(980) \rightarrow \pi^+\pi^-$ mainly couples with $f_0(980)$, $f_0(1710)$,

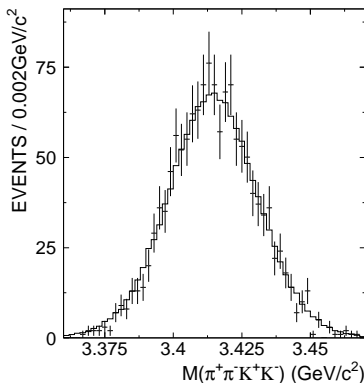


FIG. 2: $\pi^+\pi^-K^+K^-$ invariant mass distributions from the 4-C fit after requiring $\text{Prob}_{5C} > 0.01$, where the error points are data and the histogram is MC.

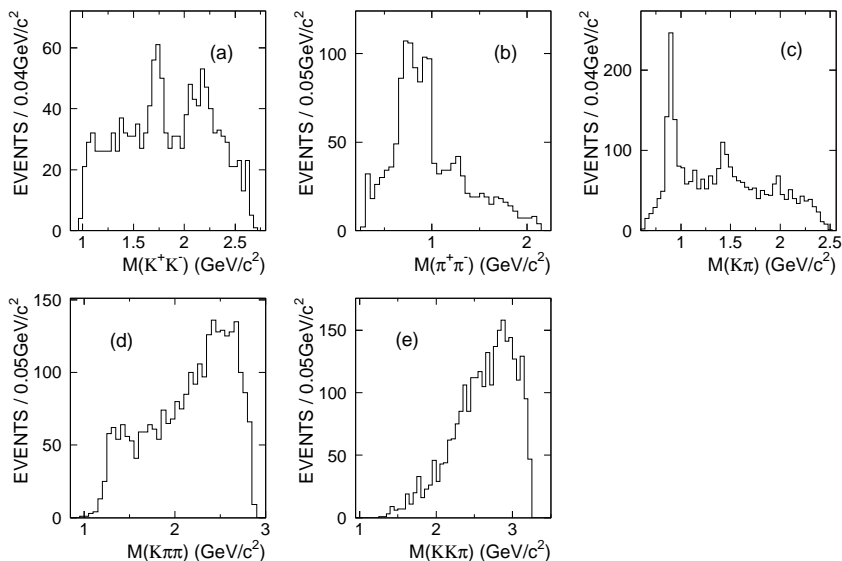


FIG. 3: The individual (a) K^+K^- , (b) $\pi^+\pi^-$, (c) $K\pi$, (d) $K\pi\pi$, and (e) $KK\pi$ invariant mass distributions after application of all selection criteria.

and $f_0(2200)$, which decay to K^+K^- , and the concentration of events at large K^+K^- mass is also associated with $\rho(770)$ decays to $\pi^+\pi^-$.

Figure 4(b) shows the scatter plot of $K^+\pi^-$ versus $K^-\pi^+$ invariant masses. There are obvious clusters due to $K^*(892)^0$ and around $1.43 \text{ GeV}/c^2$, where there are several known resonances, and evidence for $(K\pi)$ structures at about $1.7 \text{ GeV}/c^2$ and $1.95 \text{ GeV}/c^2$, as well as an enhancement above $2 \text{ GeV}/c^2$. There is also a possible small accumulation outside the $K^*(892)^0\bar{K}^*(892)^0$ cluster, which may be due to the broad S-wave structure κ .

The $K\pi\pi$ mass distributions for events where one $K^\pm\pi^\mp$ combination is in the $K^*(892)$ mass region $896 \pm 60 \text{ MeV}/c^2$ and where the $\pi^+\pi^-$ mass in the $\rho(770)$ mass range from 700 to $850 \text{ MeV}/c^2$ are shown in Fig. 5. Strong $K_1(1270)$ signals are observed in both cases, and there is also a weak peak around $1.4 \text{ GeV}/c^2$ for the $K^*\pi$ decay mode.

IV. ANALYSIS METHOD

We have carried out a partial wave analysis using relativistic covariant tensor amplitudes constructed from Lorentz-invariant combinations of the four-vectors and the photon polarization for $\psi(2S)$ initial states with helicity ± 1 [8, 9]. For $\psi(2S) \rightarrow \gamma\chi_{c0}$, $\chi_{c0} \rightarrow \pi^+\pi^-K^+K^-$, the general form for the decay amplitude is

$$A = \psi_\mu(m_1)e_\nu^*(m_2)A^{\mu\nu} = \psi_\mu(m_1)e_\nu^*(m_2) \sum_i \Lambda_i U_i^{\mu\nu},$$

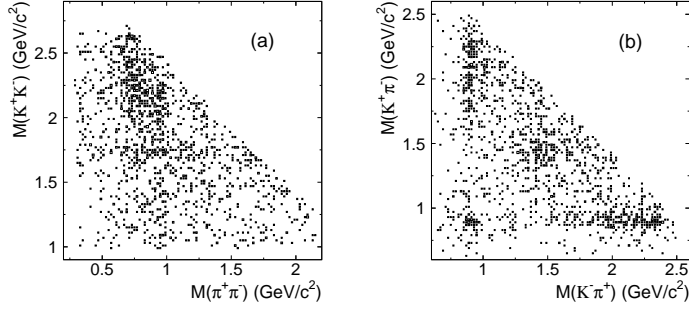


FIG. 4: The scatter plots of (a) K^+K^- versus $\pi^+\pi^-$ and (b) $K^+\pi^-$ versus $K^-\pi^+$ invariant mass for selected $\psi(2S) \rightarrow \gamma\chi_{c0}, \chi_{c0} \rightarrow \pi^+\pi^-K^+K^-$ events.

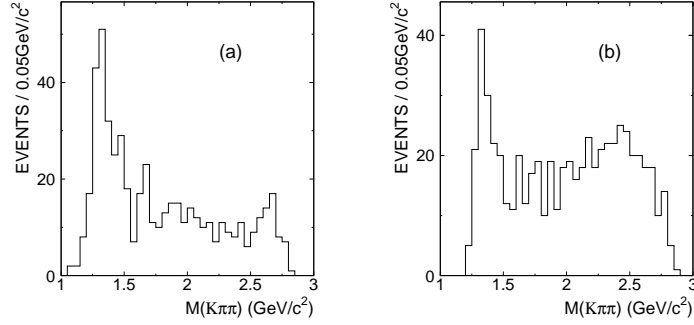


FIG. 5: $K\pi\pi$ mass distributions for events where (a) one $K^\pm\pi^\mp$ combination is in the mass region $896 \pm 60 \text{ MeV}/c^2$ and (b) the $\pi^+\pi^-$ mass is in the range $700 - 850 \text{ MeV}/c^2$.

where $\psi_\mu(m_1)$ is the $\psi(2S)$ polarization four-vector, $e_\nu(m_2)$ is the polarization four-vector of the photon, and $U_i^{\mu\nu}$ is the partial wave amplitude with coupling strength determined by a complex parameter Λ_i . For the photon polarization four-vector e_ν with photon momentum q , there is the usual Lorentz orthogonality condition $e_\nu q^\nu = 0$. We assume the Coulomb gauge in the $\psi(2S)$ rest system with momentum p_ψ , i.e., $e_\nu p_\psi^\nu = 0$. Then we have

$$\sum_{m_2} e_\nu^*(m_2) e_{\nu'}(m_2) = -g_{\nu\nu'} + \frac{q_\nu K_{\nu'} + K_\nu q_{\nu'}}{q \cdot K} - \frac{K \cdot K}{(q \cdot K)^2} q_\nu q_{\nu'} \equiv -g_{\nu\nu'}^{(\perp\perp)}$$

with $K = p_\psi - q$ and $e_\nu K^\nu = 0$. We know that

$$\sum_{m_1=1}^2 \psi_\mu(m_1) \psi_{\mu'}^*(m_1) = \delta_{\mu\mu'} (\delta_{\mu 1} + \delta_{\mu 2}),$$

so the radiative decay cross section is:

$$\begin{aligned} \frac{d\sigma}{d\Phi} &= \frac{1}{2} \sum_{m_1=1}^2 \sum_{m_2=1}^2 \psi_\mu(m_1) e_\nu^*(m_2) A^{\mu\nu} \psi_{\mu'}^*(m_1) e_{\nu'}(m_2) A^{*\mu'\nu'} \\ &= -\frac{1}{2} \sum_{i,j} \Lambda_i \Lambda_j^* \sum_{\mu=1}^2 U_i^{\mu\nu} g_{\nu\nu'}^{(\perp\perp)} U_j^{*\mu'\nu'} \equiv \sum_{i,j} P_{ij} \cdot F_{ij} \end{aligned}$$

where

$$\begin{aligned} P_{ij} &= P_{ji}^* = \Lambda_i \Lambda_j^*, \\ F_{ij} &= F_{ji}^* = -\frac{1}{2} \sum_{\mu=1}^2 U_i^{\mu\nu} g_{\nu\nu'}^{(\perp\perp)} U_j^{*\mu'\nu'}. \end{aligned}$$

The partial wave amplitudes U_i for the intermediate states used in the analysis, such as the $K^*(892)^0 \bar{K}^*(892)^0$ are constructed with the four-momenta of the π^+ , π^- , K^+ , and K^- , and their specific expressions are given in Ref. [9]. For an intermediate resonance, the corresponding Breit-Wigner propagator is denoted by a function:

$$BW = \frac{1}{M^2 - s - iM\Gamma},$$

where s is the invariant mass-squared and M , Γ are the resonance mass and width. Angular momenta L up to 2 in the production process are needed, but higher L give negligible contributions. Standard Blatt-Weisskopf centrifugal barrier factors [8, 9] are included using a radius of interaction of 0.8 fm, though results are insensitive to this radius.

The relative magnitudes and phases of the amplitudes are determined by an unbinned maximum likelihood fit. The basis of likelihood fitting is calculating the probability that a hypothesized probability distribution function (PDF) would produce the data set under consideration. If the probability to produce event i , characterized by the measurements x_i , is $P(x_i)$, then the joint probability density for observing the N events in the data sample is

$$\mathcal{L} = \prod_{i=1}^N P(x_i).$$

The normalization condition for $P(x_i)$ is that its integral over its domain must not depend on the values of the fit parameters. Suppose the differential cross section $\left(\frac{d\sigma}{d\Phi}\right)_i$ is the unnormalized PDF for producing event i . Then

$$P(x_i) = \frac{\left(\frac{d\sigma}{d\Phi}\right)_i}{\int \left(\frac{d\sigma}{d\Phi}\right) d\Phi},$$

where the integration is over the domain of $\left(\frac{d\sigma}{d\Phi}\right)$.

For the purpose of normalizing the PDF used in fitting the experimental data set, several million MC $\psi(2S) \rightarrow \gamma\chi_{c0}$, $\chi_{c0} \rightarrow \pi^+\pi^-K^+K^-$ phase space events were generated. The events undergo detector simulation and are passed through the same analysis procedure as are the experimental data, and thus the distribution of the MC events passing into the final stage of analysis contains the acceptance information. The normalization integral is then computed as:

$$\int \left(\frac{d\sigma}{d\Phi}\right) d\Phi = \sigma \rightarrow \frac{1}{N_{MC}} \sum_{i'=1}^{N_{MC}} \left(\frac{d\sigma}{d\Phi}\right)_{i'} = \frac{1}{N_{MC}} \sum_{i'=1}^{N_{MC}} \left(\sum_{j,k} P_{jk} \cdot F_{jk} \right)_{i'},$$

where N_{MC} is the number of accepted MC events.

Background events obtained from MC simulation are included in the fit, but with the opposite sign of log likelihood compared to data. These events are used to cancel the backgrounds within the data sample in the maximum likelihood fit. This technique of background treatment has been used in analyses of Crystal Barrel data (see Ref. [10]) and several previous BESII publications [11, 12, 13]. Then finally we have the logarithm of \mathcal{L}

$$\ln \mathcal{L} = \sum_{i=1}^{N'} \ln \left[\frac{\left(\frac{d\sigma}{d\Phi}\right)_i}{\sigma} \right] = \sum_{i=1}^{N'} \ln \left[\frac{\left(\sum_{j,k} P_{jk} \cdot F_{jk} \right)_i}{\frac{1}{N_{MC}} \sum_{i'=1}^{N_{MC}} \left(\sum_{j,k} P_{jk} \cdot F_{jk} \right)_{i'}} \right],$$

where N' is the total number of data and background events.

For the $\psi(2S) \rightarrow \gamma\chi_{c0}$, $\chi_{c0} \rightarrow \pi^+\pi^-K^+K^-$ process, small backgrounds remaining arise mainly from $\psi(2S) \rightarrow \pi^0\pi^+\pi^-K^+K^-$, $\psi(2S) \rightarrow \pi^0\pi^+\pi^-\pi^+\pi^-$, $\psi(2S) \rightarrow \gamma\chi_{c0}$, $\chi_{c0} \rightarrow \pi^+\pi^-\pi^+\pi^-$, $\psi(2S) \rightarrow \gamma\chi_{c1}$, $\chi_{c1} \rightarrow \pi^+\pi^-K^+K^-$, and $\psi(2S) \rightarrow \gamma\chi_{c0}$, $\chi_{c0} \rightarrow K_S^0 K^\pm \pi^\mp$. The number of background events is estimated to be about 29, only a few percent of the data sample, from detailed exclusive and inclusive MC simulations, and therefore the effect of background is expected to be minor in the partial wave analysis. In the MC simulation we increase the amount of background by a factor of 10 and then multiply by a normalization factor of 0.1 to reduce the statistical fluctuation of the background events.

The optimization of the free parameters Λ_i within the amplitude is done using FUMILI [14], which also gives the fitting error matrix. Technically, rather than maximizing $\ln \mathcal{L}$, this package minimizes $S = -\ln \mathcal{L}$. In the minimizing procedure, a change in log likelihood of 0.5 represents a one standard deviation effect.

V. ANALYSIS RESULTS

Table I shows the decay modes considered in the partial wave analysis, which are motivated by the structures seen in the scatter plots of Figs. 4(a) and (b) and in projections of Figs. 3 and 5, changes ΔS in log likelihood when the component is dropped from the fit, and the corresponding statistical significances. The partial wave amplitude improves log likelihood by more than 5 in most cases. The decay modes $f_0(980)f_0(1710)$, $f_2(1270)f_2(1270)$, and $f_0(1710)f_0(1370)$, where for the latter $f_0(1710)$ decays to $\pi^+\pi^-$ and $f_0(1370)$ decays to K^+K^- , are shown for completeness, but they are not very significant. The significances are calculated from comparing the difference between the S values of the fits with and without the component.

TABLE I: Decay modes fitted in the partial wave analysis, changes ΔS in log likelihood when the component is dropped from the fit, and the corresponding statistical significances. The errors are statistical only.

Decay mode	Fitted events	ΔS	Significance
$(\pi^+\pi^-)(K^+K^-)$			
$f_0(980)f_0(980)$	27.9 ± 8.7	15.7	5.3σ
$f_0(980)f_0(1710)$	14.7 ± 7.0	5.2	2.8σ
$f_0(980)f_0(2200)$	77.1 ± 13.0	27.3	7.1σ
$f_0(1370)f_0(980)$	26.9 ± 10.0	14.6	5.0σ
$f_0(1370)f_0(1710)$	60.6 ± 15.7	23.5	6.5σ
$f_2(1270)f_2(1270)$	5.9 ± 4.1	5.8	3.0σ
$\sigma f_0(1710)$	46.7 ± 13.4	22.2	6.3σ
$\sigma f_0(2200)$	23.9 ± 8.8	8.5	3.7σ
$f_0(1710)f_0(1370)$	4.6 ± 4.9	2.5	1.7σ
$(K^+\pi^-)(K^-\pi^+)$			
$K^*(892)^0 K^*(892)^0$	64.5 ± 13.5	31.1	7.1σ
$K^*(892)^0 \bar{K}^*(1680)^0 + c.c.$	40.5 ± 13.3	21.0	5.6σ
$K_0^*(1430) \bar{K}_0^*(1430)$	82.9 ± 18.8	28.0	7.2σ
$K_2^*(1430) \bar{K}_2^*(1430)$	9.2 ± 5.3	7.1	3.3σ
$K_0^*(1430) \bar{K}_2^*(1430) + c.c.$	62.0 ± 12.1	40.6	8.7σ
$K_0^*(1430) \bar{K}_0^*(1950) + c.c.$	71.0 ± 19.1	22.7	6.4σ
$\kappa \bar{\kappa}$	106.8 ± 16.7	39.2	8.6σ
$K^*(892)^0 \bar{K}^*(2300)^0 + c.c.$	115.7 ± 19.4	45.2	8.8σ
$(K^\pm \pi^+ \pi^-) K^\mp$			
$K_1(1270)^+ K^- + c.c.$	153.0 ± 19.5	102.2	13.2σ
$K_1(1400)^+ K^- + c.c.$	19.7 ± 8.9	6.9	2.7σ
$K(1460)^+ K^- + c.c.$	79.7 ± 16.8	39.3	8.2σ

The statistical uncertainties on the measurements shown in Table I are derived from the uncertainties in the fitting parameters. Recall that the parameters used in the fitting function are magnitudes and phases of the various processes. The numbers of events are derived from the parameters using numerical integration of the individual amplitudes. Using the numerical expression of the total cross section σ defined in section IV, the number of fitted events, N_i for an intermediate decay which has one partial wave amplitude U_i , is given by the integral over phase space (i.e. the sum over the MC events) of the PDF for that decay:

$$N_i = \frac{1}{N_{MC}} \sum_{i'=1}^{N_{MC}} \left(P_{ii} \cdot F_{ii} \right)_{i'} \cdot N'' ,$$

where N'' is the number of events after background subtraction. For the intermediate decay with two partial wave amplitudes U_i , U_j , we replace $P_{ii} \cdot F_{ii}$ with $P_{ii} \cdot F_{ii} + P_{ij} \cdot F_{ij} + P_{ji} \cdot F_{ji} + P_{jj} \cdot F_{jj}$, where $P_{ij} \cdot F_{ij}$ and $P_{ji} \cdot F_{ji}$ correspond to the interference terms; and those with more amplitudes can be deduced similarly.

A numerical scheme is used to extract the uncertainties on the numbers of fitted events. The standard deviations and the covariances of the fit parameters are obtained from FUMILI. Next, taking into account the correlation coefficients, a thousand sets of fit parameters are generated using a random number generator CORGEN [15]. These random numbers are distributed as correlated Gaussian distributions. The number of fitted events for each process is then calculated with each of the thousand sets of parameters, and histogrammed. A Gaussian function is then fit to each of these histograms, and the standard deviations are determined.

The mass projections in K^+K^- , $\pi^+\pi^-$, $K\pi$, and $K\pi\pi$ are shown in Fig. 6. There is a reasonable agreement between the data and the fit.

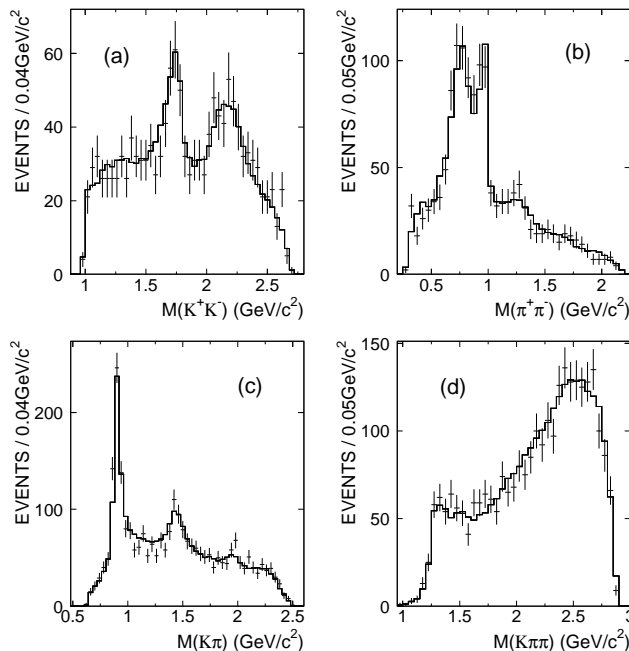


FIG. 6: Mass projections on (a) K^+K^- , (b) $\pi^+\pi^-$, (c) $K\pi$ and (d) $K\pi\pi$ for $\psi(2S) \rightarrow \chi_{c0}$, $\chi_{c0} \rightarrow \pi^+\pi^-K^+K^-$. The histograms represent the fit result, and the points with error bars are data.

A. $\chi_{c0} \rightarrow (\pi^+\pi^-)(K^+K^-)$

We begin by discussing the $\chi_{c0} \rightarrow (\pi^+\pi^-)(K^+K^-)$ decay modes. In Fig. 6(b), the $\rho(770)$ due to the decay of $K_1(1270) \rightarrow K\rho(770)$ and a strong $f_0(980)$ are observed. Along the $f_0(980) \rightarrow \pi^+\pi^-$ band in Fig. 4(a), there are several enhancements, one at the K^+K^- threshold and others around 1.75 GeV/c^2 and 2.2 GeV/c^2 , which correspond to the $f_0(980)f_0(980)$, $f_0(980)f_0(1710)$, and $f_0(980)f_0(2200)$ modes listed in Table I.

In the fit, the $f_0(980)$ is described with the usual Flatté formula [16, 17], and the parameters used are those of Ref. [17]. At higher $\pi^+\pi^-$ mass, a weak signal around 1.3 GeV/c^2 is visible. It is mainly from couplings of the $f_0(1370)$ with $f_0(980)$ and $f_0(1710)$ which decay to K^+K^- . A free fit to $f_0(1370)$ gives a fitted mass of 1265 ± 30 MeV/c^2 and a width of 350 ± 100 MeV/c^2 with large statistical errors. Apart from the above structures, a correlation between the low $\pi^+\pi^-$ mass enhancement and K^+K^- mass greater than 1.5 GeV/c^2 also appears in Fig. 4(a). We describe it by adding $\sigma f_0(1710)$ and $\sigma f_0(2200)$ decay modes, where the parameterization of a $J/\psi \rightarrow \omega\pi^+\pi^-$ analysis (Adler zero parameterization) [12] is adopted to describe the broad S-wave σ . The $\sigma f_0(1710)$ and $f_0(1370)f_0(1710)$ decays dominate the production of $f_0(1710)$ in the partial wave fit of $\psi(2S) \rightarrow \gamma\chi_{c0}$, $\chi_{c0} \rightarrow \pi^+\pi^-K^+K^-$.

The fitted mass and width of the $f_0(1710)$ are $M = 1760 \pm 15$ MeV/c^2 and $\Gamma = 125 \pm 25$ MeV/c^2 . The mass is somewhat higher than the PDG value [1]. The $f_0(1790)$ has been recently claimed in J/ψ decays [13]. The parameters of $f_0(1790)$ and those of $f_0(1710)$ given by the PDG and Ref. [11] are tested in this analysis, and the log likelihood becomes worse by 10.3, 11.5, and 4.2, respectively. The log likelihood can be improved by 5.7 if both the $f_0(1790)$ and $f_0(1710)$ (using parameters of Ref. [11]) are included into the fit, while the results for the other components only change a little. A fit replacing the decay modes with an $f_0(1710)$ with $f_2(1710)$ – namely, using $\sigma f_2(1710)$, $f_0(980)f_2(1710)$, and $f_0(1370)f_2(1710)$ decays instead of $\sigma f_0(1710)$, $f_0(980)f_0(1710)$, and $f_0(1370)f_0(1710)$ in the fit – is made in order to check the spin-parity of the structure around 1.75 GeV/c^2 in the K^+K^- mass region. It gives a worse log likelihood by 55.6 and a poor fit result, as shown in Fig. 7(a).

There are two ρ -like resonances, $\rho(1450)$ and $\rho(1700)$, which decay to $K\bar{K}$ final states in the 1600- MeV/c^2 region [1]. As a check, we add $\rho(770)\rho(1450)$ and $\rho(770)\rho(1700)$ intermediate decay modes into the fit with four more fitted parameters, using the mass and width measurements given by Ref. [18], and the log likelihood is improved by 6.4. Replacing the components $\sigma f_0(1710)$, $f_0(980)f_0(1710)$, and $f_0(1370)f_0(1710)$ with $\rho(770)\rho(1450)$ and $\rho(770)\rho(1700)$ gives a worse log likelihood by 81.6, and the corresponding fit is shown in Fig. 7(b). An investigation of the $\rho(770)$

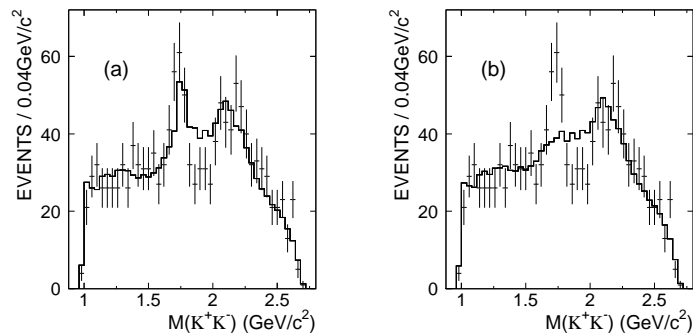


FIG. 7: Mass projections in K^+K^- for fits replacing $f_0(1710)$ with (a) $f_2(1710)$ or (b) $\rho(1450)$ and $\rho(1700)$. The dots with error bars are data, and the histograms are the fits.

band in Fig. 4(a) indicates that the structures at high K^+K^- mass are a reflection of the other intermediate decay modes.

A free fit to $f_0(2200)$ gives a fitted mass of 2170 ± 20 MeV/ c^2 and a width of 220 ± 60 MeV/ c^2 . There are several scalar and tensor resonances located in the mass range greater than 2.0 GeV/ c^2 which decay to the K^+K^- final states [1]: $\rho(2150)$, $f_2(2150)$, $f_0(2200)$, and $f_2(2300)$. A variety of alternative fits to the high K^+K^- mass region, listed in Table II, using these resonances and the $f_0(2100)$ have been tried. Note that PDG mass and width values [1] are used in the fits for the $f_0(2100)$, $f_2(2150)$, $\rho(2150)$, and $f_2(2300)$ and that $f_0(2100)$, $f_2(2150)$, $f_0(2200)$, and $f_2(2300)$ couple with the σ and $f_0(980)$, while the $\rho(2150)$ couples with the $\rho(770)$. We also tried $f_2(2200)$ instead of the $f_0(2200)$ in one fit, assuming it couples with the σ and $f_0(980)$.

TABLE II: Alternative fits to the high K^+K^- mass region instead of using only a $f_0(2200)$ involved in the fit; the right-hand column shows values of ΔS ; positive values indicate poorer fits.

Components	ΔS
a) $\rho(2150)$	+35.3
b) $f_2(2200)$ $M = 2170$ MeV/ c^2 , $\Gamma = 220$ MeV/ c^2	+33.1
c) $f_2(2150) + f_0(2200)$	-4.5
d) $f_2(2150) + f_0(2100)$	+9.9
e) $f_2(2150) + f_2(2300)$	+28.6
f) $f_0(2100) + f_0(2200)$	-4.3
g) $f_0(2100) + f_2(2300)$	-3.5
h) $f_0(2200) + f_2(2300)$	-9.0
i) $f_2(2150)$	+32.5

In Table II, fit a), using $\rho(770)\rho(2150)$ instead of $\sigma f_2(2200)$ and $f_0(980)f_0(2200)$, gives a worse log likelihood by 35.3. A fit with both $f_0(2200)$ and $\rho(2150)$ improves the log likelihood by about 3.0 compared to the case with $f_0(2200)$ only. Also b), e), and i), where no scalar is included, as well as d), give bad fits. Fits c), f), g), and h) improve the log likelihood a little, but not significantly.

Based on these fit results, we conclude that a scalar state $f_0(2200)$ at about 2.2 GeV/ c^2 which decays to K^+K^- is needed in this channel, but no additional significant 0^{++} or 2^{++} is required in this mass region according to our study in Table II.

B. $\chi_{c0} \rightarrow (K^+\pi^-)(K^-\pi^+)$

The shape of the $K^*(892)$ is described by a P-wave relativistic Breit-Wigner curve, with a width

$$\Gamma = \Gamma_0 \frac{m_0}{m} \frac{1 + r^2 p_0^2}{1 + r^2 p^2} \left[\frac{p}{p_0} \right]^3,$$

where m is the mass of the $K\pi$ system, p is the momentum of kaon in the $K\pi$ system, Γ_0 is the width of the resonance, m_0 is the mass of the resonance, p_0 is p evaluated at the resonance mass, r is the interaction radius and $\frac{1+r^2p_0^2}{1+r^2p^2}$ represents the contribution of the barrier factor. The value $(3.4 \pm 0.6 \pm 0.3)$ (GeV/c) $^{-1}$ measured by the $K^-\pi^+$ scattering experiment [19] as an approximate estimation of the interaction radius r is used.

Adding a $K^*(892)^0\bar{K}^*(1680)^0$ decay mode improves log likelihood by 21.0, where the mass and width of $K^*(1680)^0$ are fixed to PDG values [1] and the interaction radius r in the fit is set to the value 2.0 given by Ref. [19].

Most of the peak at 1430 MeV/c 2 is fitted as $K_0^*(1430)\bar{K}_0^*(1430)$ and $K_0^*(1430)\bar{K}_2^*(1430) + c.c.$, with only a small contribution from $K_2^*(1430)\bar{K}_2^*(1430)$ – the fitted number of $K_2^*(1430)\bar{K}_2^*(1430)$ events is about 11% of that of $K_0^*(1430)\bar{K}_0^*(1430)$. Adding the $K_2^*(1430)\bar{K}_2^*(1430)$ mode improves the log likelihood by 7.1, which corresponds to about a significance of 3.3σ for two free parameters of the fitted amplitudes. The mass and width of the $K_2^*(1430)$ are fixed to the PDG values [1]. A free fit to $K_0^*(1430)$ gives a fitted mass of 1455 ± 20 MeV/c 2 and a width of 270 ± 45 MeV/c 2 .

There is another structure visible around 1.95 GeV/c 2 in the $K\pi$ mass distribution. Among the three generalized C-parity allowed intermediate decays from χ_{c0} , $K_0^*(1430)\bar{K}_0^*(1950)$, $K_2^*(1430)\bar{K}_0^*(1950)$, and $\kappa\bar{K}_0^*(1950)$, the first decay gives a better log likelihood value in our fit than the other two by 22.9 and 14.6, respectively. A free fit gives a fitted mass of 1945 ± 30 MeV/c 2 , but the width is poorly determined, ~ 500 MeV/c 2 , so we adopt the PDG mass and width values for the $K_0^*(1950)$ in the partial wave analysis.

In Fig. 4(b) there is a possible accumulation outside the $K^*(892)^0\bar{K}^*(892)^0$ cluster. Its explanation may be the broad S-wave κ . Since the properties of κ are still controversial (cf., the review paper in the PDG [1], and references therein), we use a Breit-Wigner amplitude of constant width, without any phase space factor with the parameterization obtained in Ref. [20], $M = 790$ MeV/c 2 , $\Gamma = 860$ MeV/c 2 to describe this broad structure. The log likelihood becomes worse by 39.2 after removing the $\kappa\bar{\kappa}$ from the fit, and the corresponding projection in $K\pi$ mass, shown in Fig. 8, obviously disagrees with data at low $K\pi$ mass.

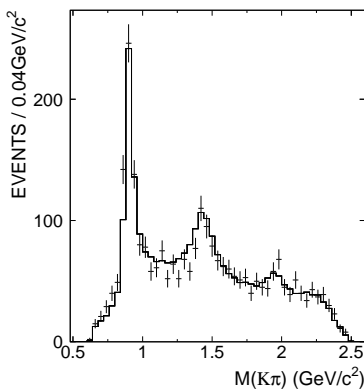


FIG. 8: The $K\pi$ mass projection for the fit without $\kappa\bar{\kappa}$ decay.

Finally, an intermediate decay mode $K^*(892)^0\bar{K}^*(2300)^0$ is added into the fit. Here the $K^*(2300)^0$ is used as an effective structure to describe the poorly known high $K\pi$ mass region. The log likelihood changes by 45.2 if the $K^*(892)^0\bar{K}^*(2300)^0$ is omitted. The scanned mass and width for $K^*(2300)^0$ are ~ 2.3 GeV/c 2 and 300 MeV/c 2 respectively. No higher spin-parity tests such as 3^- or 5^- are made.

C. $\chi_{c0} \rightarrow (K^\pm\pi^+\pi^-)K^\mp$

In Fig. 5 there are strong $K_1(1270)$ signals in both $K\rho(770)$ and $K^*(892)\pi$, and there is also a weak peak around 1.4 GeV/c 2 in the $K^*(892)\pi$. In the partial wave analysis, $K_1(1270)K$ and $K_1(1400)K$ decays, where $K_1(1270)$ decays to $K\rho(770)$, $K^*(892)\pi$, and $K_0^*(1430)\pi$ and $K_1(1400)$ decays to $K^*(892)\pi$, are added. The fit also requires an additional structure to describe the $K\pi\pi$ mass distribution at about 1.4 GeV/c 2 . Here adding $K(1460)$ in the fit will improve the log likelihood by 39.3; in the fit, the mass and width values given by the PDG [1] are used. The masses and widths of the $K_1(1270)$ and $K_1(1400)$ are also fixed to PDG values so as to reduce uncertainties.

There are two lowest-lying axial-vector-meson octets. These correspond to the singlet (1P_1) and triplet (3P_1) spin configurations of two quarks in a P-wave orbital angular momentum state. The nonstrange, isospin $I = 1$ members of the two octets have opposite G parity: the $b_1(1235)$ is in the 1P_1 octet and has $G = +1$, while the $a_1(1260)$ is in the 3P_1 octet and has $G = -1$. The strange members of the 3P_1 and 1P_1 octets, the K_A and K_B , respectively, are

mixtures of the observed physical states, the $K_1(1270)$ and the $K_1(1400)$, where

$$\begin{aligned} K_A &= \cos\theta K_1(1400) + \sin\theta K_1(1270), \\ K_B &= \cos\theta K_1(1270) - \sin\theta K_1(1400), \end{aligned}$$

and the mixing angle is near $\theta \simeq 45^\circ$ [21]. The dominant $K_1(1270)$ decay mode is to $K\rho(770)$ ($\mathcal{B} = 42\% \pm 6\%$); the $K_1(1400)$ decays almost always to $K^*(892)\pi$ ($\mathcal{B} = 94\% \pm 6\%$). In the limit of strict flavor SU(3) symmetry, the amplitudes for two-body decays to conjugate mesons in the same pair of octets should be equal. Thus, since decays to $b_1\pi$ are forbidden by G parity, decays to $K_B\bar{K}$ are disallowed by SU(3), and one expects relatively pure $K_A\bar{K}$ final states in χ_{c0} decays. And, since $\theta \simeq 45^\circ$, there should be roughly equal amounts of $K_1(1270)$ and $K_1(1400)$.

The remarkable feature of the $K\pi\pi$ distribution is that the contribution of the $K_1(1400)$ in the final fit is very small compared to the large $K_1(1270)$ signal. Adding a $K_1(1400)$ improves the log likelihood by 6.9 which corresponds to the significance of about 2.7σ . The partial wave analysis yields a $K_1(1270) \rightarrow K\rho(770)$ signal of 68.3 ± 13.4 events and a $K_1(1400) \rightarrow K^*(892)\pi$ signal of 19.7 ± 8.9 events. The function used to fit the $K_1(1270)$ is a convolution of an S-wave Breit-Wigner function for the $K_1(1270)$ with a P-wave Breit-Wigner function for the $\rho(770)$ meson. Flavor-SU(3)-violating $K_1(1270) - K_1(1400)$ asymmetry for χ_{c0} decay is observed.

D. GOODNESS-OF-FIT

To determine the goodness of fit, a χ^2 is calculated by comparing histograms, *e.g.*, a vector of Poisson distributed numbers $\mathbf{n} = (n_1, \dots, n_N)$, with a hypothesis for their expectation values $\nu_i = E[n_i]$. As the distribution is Poisson with variances $\sigma_i^2 = \nu_i$, the χ^2 becomes *Pearson's χ^2 statistic*,

$$\chi^2 = \sum_{i=1}^N \frac{(n_i - \nu_i)^2}{\nu_i}.$$

If the hypothesis $\nu = (\nu_1, \dots, \nu_N)$ is correct and if the measured values n_i are sufficiently large, then the χ^2 statistic will follow the χ^2 probability density function with the number of degrees of freedom (ndf) equal to the number of measurements N minus the number of fitted parameters.

For an n -body final state, the number of independent kinematic variables is $3n - 4$. Thus, one can compare $3n - 4$ selected independent variables with the fit results by defining a quantity

$$\chi_{all}^2 = \sum_{j=1}^{3n-4} \chi_j^2$$

to check the quality of a global fit, which obeys the χ^2 distribution approximately with the number of degrees of freedom equal to the total number of measurements minus the number of fitted parameters; and the individual χ_j^2 will give a qualitative measure of the goodness of fit for each kinematic variable.

The number of independent kinematic variables for $\psi(2S) \rightarrow \gamma\chi_{c0}$, $\chi_{c0} \rightarrow \pi^+\pi^-K^+K^-$ process is 10 after the use of the 5-C fit with the additional χ_{c0} mass constraint. We use the following 10 distributions to check the goodness-of-fit:

- $(\theta, \phi)_{\pi\pi KK}$ = the polar angle and azimuthal angle of the $(\pi^+\pi^-K^+K^-)$ in the laboratory system,
- $(\theta, \phi)_{\pi\pi K}$ = the polar angle and azimuthal angle of the $(\pi^+\pi^-K^-)$ in the $(\pi^+\pi^-K^+K^-)$ center of mass,
- $(\theta, \phi)_{\pi K}$ = the polar angle and azimuthal angle of the (π^+K^-) in the $(\pi^+\pi^-K^-)$ center of mass,
- $(\theta, \phi)_\pi$ = the polar angle and azimuthal angle of the π^+ in the (π^+K^-) center of mass,

and the invariant masses for the $(\pi^+\pi^-K^-)$ and (π^+K^-) systems. Table III shows the results, where the number of bins is taken as the number of degrees of freedom for each individual distribution, and Fig. 9 shows the projections of the 10 variables. There is excellent agreement between the data and fit.

Using the results in Table III, the χ_{all}^2 obtained is 219.8 with 185 degrees of freedom (=237-52, where 237 is a sum of the bin numbers for the 10 distributions and 52 is the number of fitted amplitude parameters), which corresponds to a confidence level of 4%.

VI. SYSTEMATIC ERROR

In this analysis, the systematic errors are estimated by considering the following sources:

TABLE III: Check of goodness of fit using 10 independent kinematic variables, where ndf and C.L. are the number of degrees of freedom and the corresponding confidence level.

Variable	χ^2	ndf	χ^2/ndf	C.L.
$\cos\theta_{\pi\pi KK}$	24.46	18	1.36	0.14
$\phi_{\pi\pi KK}$	14.23	20	0.71	0.82
$\cos\theta_{\pi\pi K}$	11.29	20	0.56	0.94
$\phi_{\pi\pi K}$	22.58	20	1.13	0.31
$\cos\theta_{\pi K}$	11.34	16	0.71	0.79
$\phi_{\pi K}$	18.81	20	0.94	0.53
$\cos\theta_{\pi}$	12.15	20	0.61	0.91
ϕ_{π}	12.63	20	0.63	0.89
$M_{\pi^+\pi^-K^-}$	37.26	36	1.04	0.41
$M_{\pi^+K^-}$	55.07	47	1.17	0.20

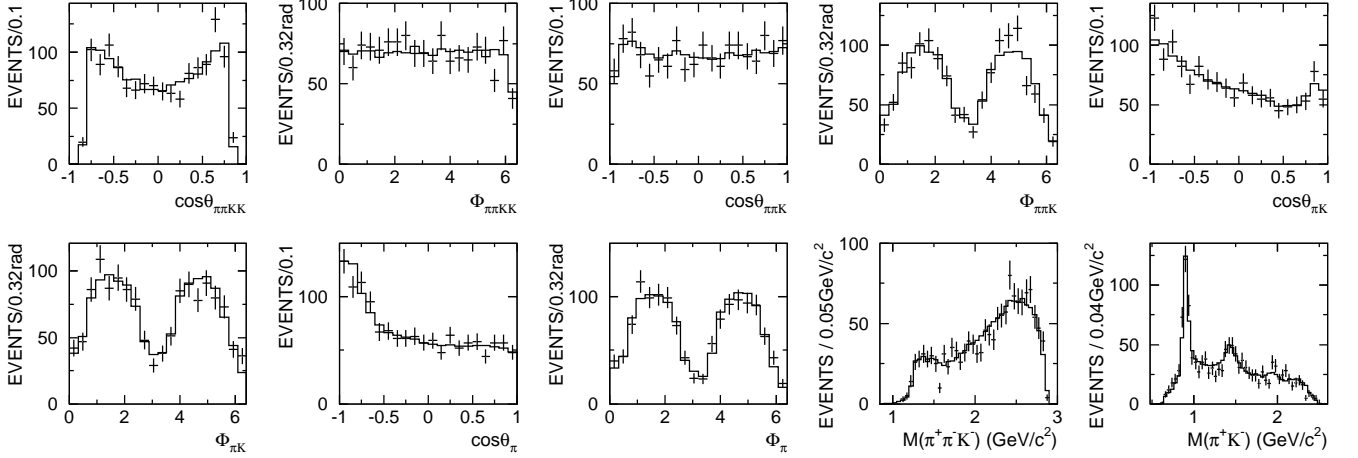


FIG. 9: Fit projections for the 10 variables described in the text after the global fit.

(1) Uncertainty of the parameterization of the σ line shape: use a Breit-Wigner amplitude of constant width $M = 470 \text{ MeV}/c^2$, $\Gamma = 613 \text{ MeV}/c^2$ [12] instead of the Adler zero parameterization.

(2) Uncertainty of the parameterization of the κ line shape: change the mass and width of the Breit-Wigner amplitude of constant width to $M = 745 \text{ MeV}/c^2$, $\Gamma = 622 \text{ MeV}/c^2$ [20].

(3) The parameters of the $f_0(980)$ are still uncertain, and in addition to the solution of Ref. [17], we also use measurements of some recent experiments such as E791, GAMS, and WA102 [22, 23, 24], where a Breit-Wigner description with the width varying from 44 to 80 MeV/c^2 was used for the $f_0(980)$. We determine the change both by using the solutions of Refs. [22, 23, 24] and by varying g_1 in Ref. [17] from 0.1108 GeV/c^2 to 0.090 GeV/c^2 and 0.130 GeV/c^2 while keeping the ratio g_2/g_1 fixed.

(4) As mentioned above, we use the measurement of Ref. [19], $(3.4 \pm 0.6 \pm 0.3) (\text{GeV}/c)^{-1}$ for r in the P-wave relativistic Breit-Wigner parameterization. We also use r varied by one sigma to 2.73 $(\text{GeV}/c)^{-1}$ and 4.07 $(\text{GeV}/c)^{-1}$ to determine the change in the fit.

(5) Vary mass and width values of the $(K\pi)$ components $K_2^*(1430)$, $K^*(1680)$, and $K_0^*(1950)$ within the PDG errors [1].

(6) Vary mass and width values of the $(K\pi\pi)$ components $K_1(1270)$, $K_1(1400)$, and $K(1460)$ within the PDG errors [1], where the width of $K(1460)$ is changed to 200 and 300 MeV/c^2 and mass to 1.40 and 1.46 GeV/c^2 .

(7) Remove the small component $f_0(1710)f_0(1370)$ from the fit, where $f_0(1710)$ decays to $\pi^+\pi^-$ and $f_0(1370)$ decays to K^+K^- .

(8) Add three $(K\pi\pi)$ resonances $K_1(1650)$, $K_2(1770)$, and $K_2(1820)$ into the fit.

(9) Remove the $K^*(892)^0 \bar{K}^*(2300)^0 + c.c.$ decay mode from the original fit but keep (8). Tests (8) and (9) strongly affect the branching fraction measurements.

(10) Try alternative starting conditions for the maximum likelihood fit.

(11) Uncertainty of the background in the partial wave analysis fit. In order to investigate the effect of the amount

and shape of background on the results, we increased the number of background events in the fit to 55, which is the maximum estimation, fitted without background, and added an incoherent phase space background normalized to 29 events instead of fitting with the opposite sign of log likelihood for the MC background. The change on the fit results is very small, less than 5% for all the measurements.

Total errors are obtained by adding the individual errors in quadrature. For the branching fraction uncertainties, the uncertainties in MDC tracking, kinematic fitting, PID, efficiency of the photon ID, and the number of $\psi(2S)$ events [25] are also included, and the total systematic error for this part, 12%, is taken from Ref. [4].

VII. DISCUSSION

From the $\chi_{c0} \rightarrow \pi^+\pi^-K^+K^-$ decay fit results, it is found that scalar resonances have large decay fractions compared to those of tensors, and such decays provide a relatively clean laboratory in which to study the properties of the scalars $f_0(980)$, $f_0(1370)$, $f_0(1710)$, and $f_0(2200)$. There is also conspicuous production due to the $K^*(892)^0\bar{K}^*(892)^0$ and $K_0^*(1430)\bar{K}_0^*(1430)$ (and $K_0^*(1430)\bar{K}_2^*(1430) + c.c.$) pairs, and flavor-SU(3)-violating $K_1(1270) - K_1(1400)$ asymmetry is observed. Information on these states is very desirable and will be described below.

For other components in Table I, because of the low statistics ($f_2(1270)f_2(1270)$, $f_0(1710)f_0(1370)$, and $K_2^*(1430)\bar{K}_2^*(1430)$), uncertain parameters of intermediate resonances involved ($\sigma f_0(1710)$, $\sigma f_0(2200)$, $K^*(892)^0\bar{K}^*(1680)^0 + c.c.$, $K_0^*(1430)\bar{K}_0^*(1950) + c.c.$, $\kappa\bar{\kappa}$, and $K(1460)K$), and the poorly known high mass $K\pi$ region which is described by the $K^*(892)^0\bar{K}^*(2300)^0 + c.c.$, it is difficult to obtain precise quantitative results or make definite conclusions. The systematic errors on the numbers of events for decay modes $f_0(980)f_0(1710)$ and $f_0(1370)f_0(980)$ are very large, while the significance of the $f_0(980)f_0(1710)$ is small; therefore we also will not consider these two decay modes in the following branching fraction measurements.

The numbers used in the branching fraction (or upper limit) calculations and the corresponding results are summarized in Table IV, where the first errors are statistical and the second are systematic. The value of $\mathcal{B}[\psi(2S) \rightarrow \gamma\chi_{c0}]$, $(9.22 \pm 0.11 \pm 0.46)\%$, recently measured by the CLEO experiment, is used [26]. The fit removing the $K_1(1270) \rightarrow K\rho(770)$ gives a worse log likelihood by 39.5, which corresponds to the signal significance of about 8.6σ . The 90% confidence level (C.L.) upper limit for $\chi_{c0} \rightarrow K_1(1400)\bar{K}$ is obtained by increasing the number of events by 1.28σ , where σ includes the statistical and the systematic errors added in quadrature.

TABLE IV: Summary of numbers used in the branching fraction (or upper limit) calculations and corresponding results, where X represents the intermediate decay modes, N^{fit} is the number of fitted events, and ϵ is the efficiency.

Decay mode	N^{fit}	ϵ (%)	Sys. error (%)	$\mathcal{B}[\chi_{c0} \rightarrow X \rightarrow \pi^+\pi^-K^+K^-]$ ($\times 10^{-4}$)	Significance
$f_0(980)f_0(980)$	27.9 ± 8.7	6.25 ± 0.01	$^{+55.7}_{-45.3}$	$3.46 \pm 1.08^{+1.93}_{-1.57}$	5.3σ
$f_0(980)f_0(2200)$	77.1 ± 13.0	7.09 ± 0.01	$^{+19.6}_{-27.2}$	$8.42 \pm 1.42^{+1.65}_{-2.29}$	7.1σ
$f_0(1370)f_0(1710)$	60.6 ± 15.7	6.59 ± 0.01	$^{+46.1}_{-23.6}$	$7.12 \pm 1.85^{+3.28}_{-1.68}$	6.5σ
$K^*(892)^0\bar{K}^*(892)^0$	64.5 ± 13.5	6.18 ± 0.01	$^{+28.3}_{-24.6}$	$8.09 \pm 1.69^{+2.29}_{-1.99}$	7.1σ
$K_0^*(1430)\bar{K}_0^*(1430)$	82.9 ± 18.8	6.15 ± 0.01	$^{+29.2}_{-18.2}$	$10.44 \pm 2.37^{+3.05}_{-1.90}$	7.2σ
$K_0^*(1430)\bar{K}_2^*(1430) + c.c.$	62.0 ± 12.1	5.66 ± 0.01	$^{+15.6}_{-23.4}$	$8.49 \pm 1.66^{+1.32}_{-1.99}$	8.7σ
$K_1(1270)^+K^- + c.c.$, $K_1(1270) \rightarrow K\rho(770)$	68.3 ± 13.4	5.68 ± 0.01	$^{+19.4}_{-17.6}$	$9.32 \pm 1.83^{+1.81}_{-1.64}$	8.6σ
$K_1(1400)^+K^- + c.c.$, $K_1(1400) \rightarrow K^*(892)\pi$	19.7 ± 8.9	4.94 ± 0.01	$^{+219}_{-24.5}$	< 11.9 (90% C.L.)	2.7σ

The partial wave fit provides magnitudes and phases of the different partial amplitudes, as well as the interference terms. The intensity from these amplitudes is used to weight both the complete set of generated MC events and the set which survives the selection procedure. The ratio between these two weighted sets is the efficiency.

Using the number of selected $\psi(2S) \rightarrow \gamma\chi_{c0} \rightarrow \gamma\pi^+\pi^-K^+K^-$ events, the overall efficiency determined by the method above, $(5.85 \pm 0.01)\%$, and the result of Ref. [26] we get the corresponding branching fractions after subtracting background

$$\begin{aligned} \mathcal{B}[\psi(2S) \rightarrow \gamma\chi_{c0} \rightarrow \gamma\pi^+\pi^-K^+K^-] &= (1.64 \pm 0.05 \pm 0.20) \times 10^{-3}, \\ \mathcal{B}[\chi_{c0} \rightarrow \pi^+\pi^-K^+K^-] &= (1.78 \pm 0.05 \pm 0.23) \times 10^{-2}. \end{aligned}$$

For the decay mode $\chi_{c0} \rightarrow f_0(980)f_0(980)$, each $f_0(980)$ can decay to either $\pi^+\pi^-$ or K^+K^- , so it is necessary to

divide the result in Table IV by a factor of 2 to obtain the branching fractions

$$\begin{aligned}\mathcal{B}[\psi(2S) \rightarrow \gamma\chi_{c0} \rightarrow \gamma f_0(980)f_0(980)]\mathcal{B}[f(980) \rightarrow \pi^+\pi^-]\mathcal{B}[f(980) \rightarrow K^+K^-] &= (1.59 \pm 0.50_{-0.72}^{+0.89}) \times 10^{-5}, \\ \mathcal{B}[\chi_{c0} \rightarrow f_0(980)f_0(980)]\mathcal{B}[f(980) \rightarrow \pi^+\pi^-]\mathcal{B}[f(980) \rightarrow K^+K^-] &= (1.73 \pm 0.54_{-0.78}^{+0.96}) \times 10^{-4}.\end{aligned}$$

Combining this result and that of Ref. [27], we can determine the ratio of the partial decay width of $f_0(980)$ to $\pi\pi$ to those of $\pi\pi$ and $K\bar{K}$:

$$\frac{\Gamma_{\pi\pi}}{\Gamma_{\pi\pi} + \Gamma_{K\bar{K}}} = \frac{(6.5 \pm 1.93) \times \frac{3}{2}}{(6.5 \pm 1.93) \times \frac{3}{2} + (1.59_{-0.86}^{+1.00}) \times 2} = 0.75_{-0.13}^{+0.11}.$$

The numerical factors $\frac{3}{2}$ and 2 take into account that (a) two-thirds of $\pi\pi$ decays are to $\pi^+\pi^-$ and one-third to $\pi^0\pi^0$ and (b) there are equal numbers of decays to K^+K^- and $K^0\bar{K}^0$. Here the errors are the statistical and the systematic errors added in quadrature, and for the systematic error, the common parts related to the MDC tracking, kinematic fitting, efficiency of the photon ID, and the number of $\psi(2S)$ events cancel.

There is a strong $f_0(980)f_0(2200)$ with a signal significance of 7.1σ in the $\chi_{c0} \rightarrow \pi^+\pi^-K^+K^-$ decay. The mass and width of the $f_0(2200)$ are optimized as $M = 2170 \pm 20_{-15}^{+10}$ MeV/ c^2 and $\Gamma = 220 \pm 60_{-45}^{+40}$ MeV/ c^2 , and

$$\mathcal{B}[\chi_{c0} \rightarrow f_0(980)f_0(2200)]\mathcal{B}[f_0(980) \rightarrow \pi^+\pi^-]\mathcal{B}[f_0(2200) \rightarrow K^+K^-] = (8.42 \pm 1.42_{-2.29}^{+1.65}) \times 10^{-4}.$$

Changing the spin-parity of the $f_0(2200)$ in the fit or adding an additional resonance, shows that the spin-parity of the $f_0(2200)$ is well determined and no additional resonance is needed in the $f_0(2200)$ mass region. However, compared to the nearby states $f_0(2100)$ and $f_2(2150)$, its properties are still less well known [1], and more experimental data are needed.

Another significant decay mode to $f_0(1370)f_0(1710)$ is also found with a significance of 6.5σ , where $f_0(1370)$ decays to $\pi^+\pi^-$ and $f_0(1710)$ decays to K^+K^- . The fitted mass and width of the $f_0(1710)$ are $M = 1760 \pm 15_{-10}^{+15}$ MeV/ c^2 and $\Gamma = 125 \pm 25_{-15}^{+10}$ MeV/ c^2 . The fitted mass is somewhat higher than the PDG value [1]. The spin 0 component can be separated from spin 2 clearly, and replacing $f_0(1710)$ with either of the tensors $\rho(1450)$ or $\rho(1700)$ does not give a reasonable fit to the data. A free fit to $f_0(1370)$ gives a fitted mass of $1265 \pm 30_{-35}^{+20}$ MeV/ c^2 and a width of $350 \pm 100_{-60}^{+105}$ MeV/ c^2 . The corresponding branching fraction is

$$\mathcal{B}[\chi_{c0} \rightarrow f_0(1370)f_0(1710)]\mathcal{B}[f_0(1370) \rightarrow \pi^+\pi^-]\mathcal{B}[f_0(1710) \rightarrow K^+K^-] = (7.12 \pm 1.85_{-1.68}^{+3.28}) \times 10^{-4}.$$

Besides the intermediate $(\pi^+\pi^-)(K^+K^-)$ decay modes listed in Table I, we tried the following combinations in the fit: $f_0(1370)f_0(1370)$, $f_0(1370)f_0(1500)$, $f_0(1500)f_0(1370)$, $f_0(1500)f_0(1500)$, and $f_0(1500)f_0(1710)$. None of them improved the log likelihood more than 5. So we didn't include these processes in the final solution of our fit and set upper limits at the 90% C.L.:

$$\begin{aligned}\mathcal{B}[\chi_{c0} \rightarrow f_0(1370)f_0(1370)]\mathcal{B}[f_0(1370) \rightarrow \pi^+\pi^-]\mathcal{B}[f_0(1370) \rightarrow K^+K^-] &< 2.9 \times 10^{-4}, \\ \mathcal{B}[\chi_{c0} \rightarrow f_0(1370)f_0(1500)]\mathcal{B}[f_0(1370) \rightarrow \pi^+\pi^-]\mathcal{B}[f_0(1500) \rightarrow K^+K^-] &< 1.8 \times 10^{-4}, \\ \mathcal{B}[\chi_{c0} \rightarrow f_0(1500)f_0(1370)]\mathcal{B}[f_0(1500) \rightarrow \pi^+\pi^-]\mathcal{B}[f_0(1370) \rightarrow K^+K^-] &< 1.4 \times 10^{-4}, \\ \mathcal{B}[\chi_{c0} \rightarrow f_0(1500)f_0(1500)]\mathcal{B}[f_0(1500) \rightarrow \pi^+\pi^-]\mathcal{B}[f_0(1500) \rightarrow K^+K^-] &< 0.55 \times 10^{-4}, \\ \mathcal{B}[\chi_{c0} \rightarrow f_0(1500)f_0(1710)]\mathcal{B}[f_0(1500) \rightarrow \pi^+\pi^-]\mathcal{B}[f_0(1710) \rightarrow K^+K^-] &< 0.73 \times 10^{-4}.\end{aligned}$$

From the results of the fit, the branching fraction $\mathcal{B}[\chi_{c0} \rightarrow K^*(892)^0 \bar{K}^*(892)^0 \rightarrow \pi^+\pi^-K^+K^-] = (8.09 \pm 1.69_{-1.99}^{+2.29}) \times 10^{-4}$ is obtained. Using the branching fraction of $K^*(892)^0$ to the charged $K\pi$ mode, which is taken as $\frac{2}{3}$, we get

$$\begin{aligned}\mathcal{B}[\psi(2S) \rightarrow \gamma\chi_{c0} \rightarrow \gamma K^*(892)^0 \bar{K}^*(892)^0] &= (1.68 \pm 0.35_{-0.40}^{+0.47}) \times 10^{-4}, \\ \mathcal{B}[\chi_{c0} \rightarrow K^*(892)^0 \bar{K}^*(892)^0] &= (1.82 \pm 0.38_{-0.45}^{+0.52}) \times 10^{-3}.\end{aligned}$$

The values obtained here are consistent with those in Ref. [4].

Most of the peak around a $K\pi$ mass ~ 1430 MeV/ c^2 is fitted with $K_0^*(1430)\bar{K}_0^*(1430)$ and $K_0^*(1430)\bar{K}_2^*(1430) + c.c.$, with only a small contribution from $K_2^*(1430)\bar{K}_2^*(1430)$. The measured branching fractions are

$$\begin{aligned}\mathcal{B}[\chi_{c0} \rightarrow K_0^*(1430)\bar{K}_0^*(1430)^0 \rightarrow \pi^+\pi^-K^+K^-] &= (10.44 \pm 2.37_{-1.90}^{+3.05}) \times 10^{-4}, \\ \mathcal{B}[\chi_{c0} \rightarrow K_0^*(1430)\bar{K}_2^*(1430)^0 + c.c. \rightarrow \pi^+\pi^-K^+K^-] &= (8.49 \pm 1.66_{-1.99}^{+1.32}) \times 10^{-4}.\end{aligned}$$

A free fit to $K_0^*(1430)$ gives a fitted mass of $1455 \pm 20 \pm 15$ MeV/ c^2 and a width of $270 \pm 45_{-35}^{+30}$ MeV/ c^2 . The fitted number of $K_2^*(1430)\bar{K}_2^*(1430)$ events is about 11% of that of $K_0^*(1430)\bar{K}_0^*(1430)$, and the signal significance of $K_2^*(1430)\bar{K}_2^*(1430)$ mode is about 3.3σ . These measurements are important for the study of χ_{c0} decays, as well as those of $K_0^*(1430)$ and $K_2^*(1430)$.

Using the results shown in Table IV and the branching fractions of $K_1(1270) \rightarrow K\rho(770)$ and $K_1(1400) \rightarrow K^*(892)\pi$ given by the PDG [1], we determine

$$\begin{aligned}\mathcal{B}[\chi_{c0} \rightarrow K_1(1270)^+K^- + c.c.] &= (6.66 \pm 1.31_{-1.51}^{+1.60}) \times 10^{-3}, \\ \mathcal{B}[\chi_{c0} \rightarrow K_1(1400)^+K^- + c.c.] &< 2.85 \times 10^{-3},\end{aligned}$$

at the 90% C.L.. To accommodate this, a mixing angle of $\theta > 57^\circ$ is required. A flavor-SU(3)-violating $K_1(1270) - K_1(1400)$ asymmetry is observed. The asymmetries with opposite character for $\psi(2S)$ and J/ψ decays were also observed in the BES I data [28], where for $\psi(2S)$ data, $\theta < 29^\circ$ and for J/ψ data $\theta > 48^\circ$.

VIII. SUMMARY

In summary, a partial wave analysis on $\chi_{c0} \rightarrow \pi^+\pi^-K^+K^-$ in $\psi(2S) \rightarrow \gamma\chi_{c0}$ decay is performed using a sample of 14 million $\psi(2S)$ events. From the fit we find significant contributions to the χ_{c0} decays from the channels $f_0(980)f_0(980)$, $f_0(980)f_0(2200)$, $f_0(1370)f_0(1710)$, $K^*(892)^0\bar{K}^*(892)^0$, $K_0^*(1430)\bar{K}_0^*(1430)$, $K_0^*(1430)\bar{K}_2^*(1430) + c.c.$ and $K_1(1270)K$. The mass and width of the $f_0(1710)$ are determined to be $1760 \pm 15_{-10}^{+15}$ MeV/ c^2 and $125 \pm 25_{-15}^{+10}$ MeV/ c^2 , and those of the $f_0(2200)$ are $2170 \pm 20_{-15}^{+10}$ MeV/ c^2 and $220 \pm 60_{-45}^{+40}$ MeV/ c^2 . Flavor-SU(3)-violating $K_1(1270) - K_1(1400)$ asymmetry is observed, with the mixing angle $\theta > 57^\circ$.

IX. ACKNOWLEDGMENT

We wish to thank Qiang Zhao for useful suggestions. The BES collaboration thanks the staff of BEPC for their hard efforts. This work is supported in part by the National Natural Science Foundation of China under contracts Nos. 10491300, 10225524, 10225525, 10425523, the Chinese Academy of Sciences under contract No. KJ 95T-03, the 100 Talents Program of CAS under Contract Nos. U-11, U-24, U-25, and the Knowledge Innovation Project of CAS under Contract Nos. U-602, U-34 (IHEP), the National Natural Science Foundation of China under Contract No. 10225522 (Tsinghua University), and the Department of Energy under Contract No. DE-FG02-04ER41291 (University of Hawaii).

-
- [1] S. Eidelman *et al.* (Particle Data Group), Phys. Lett. B **592**, 1 (2004).
 - [2] C. Amsler and F.E. Close, Phys. Rev. D **53**, 295 (1996).
 - [3] Mark I Collaboration, W.M. Tanenbaum *et al.*, Phys. Rev. D **17**, 1731 (1978).
 - [4] BES Collaboration, M. Ablikim *et al.*, Phys. Rev. D **70**, 092003 (2004).
 - [5] BES Collaboration, J.Z. Bai *et al.*, Nucl. Instrum. Methods Phys. Res., Sect. A **458**, 627 (2001).
 - [6] BES Collaboration, M. Ablikim *et al.*, physics/0503001.
 - [7] BES Collaboration, J.Z. Bai *et al.*, Phys. Rev. D **60**, 072001 (1999).
 - [8] B.S. Zou and D.V. Bugg, Eur. Phys. J. A **16**, 537 (2003).
 - [9] S. Dulat and B.S. Zou, hep-ph/0508087.
 - [10] A.V. Anisovich *et al.*, Phys. Lett. B **491**, 40 (2000).
 - [11] BES Collaboration, J.Z. Bai *et al.*, Phys. Rev. D **68**, 052003 (2003).
 - [12] BES Collaboration, M. Ablikim *et al.*, Phys. Lett. B **598**, 149 (2004).
 - [13] BES Collaboration, M. Ablikim *et al.*, Phys. Lett. B **607**, 243 (2005).
 - [14] I. Silin, 1971, CERN Program Library D **510**.
 - [15] F. James, 1994, CERN Program Library V **122**.
 - [16] S.M. Flatté, Phys. Lett. B **63**, 224 (1976).
 - [17] B.S. Zou and D.V. Bugg, Phys. Rev. D **48**, R3948 (1993).
 - [18] Crystal Barrel Collaboration, A. Abele *et al.*, Phys. Lett. B **468**, 178 (1999).
 - [19] D. Aston *et al.*, Nucl. Phys. B **296**, 493 (1988).
 - [20] W.G. Li, *Hadron Spectroscopy*, AIP Conf. Proc. No. 717 (AIP, Acshaffenburg, Germany, 2003), p. 495.
 - [21] See, for example, H.G. Blundell, S. Godfrey and B. Phelps, Phys. Rev. D **53**, 3712 (1996); M. Suzuki, *ibid.* **47**, 1252 (1993), and references therein.

- [22] E791 Collaboration, E.M. Aitala *et al.*, Phys. Rev. Lett. **86**, 765 (2001).
- [23] GAMS Collaboration, R. Bellazzini *et al.*, Phys. Lett. B **467**, 296 (1999).
- [24] WA102 Collaboration, D. Barberis *et al.*, Phys. Lett. B **453**, 316 (1999); **453**, 325 (1999).
- [25] X.H. Mo *et al.*, High Energy Phys. Nucl. Phys. **28**, 455 (2004).
- [26] CLEO Collaboration, S.B. Athar *et al.*, Phys. Rev. D **70**, 112002 (2004).
- [27] BES Collaboration, M. Ablikim *et al.*, Phys. Rev. D **70**, 092002 (2004).
- [28] BES Collaboration, J.Z. Bai *et al.*, Phys. Rev. Lett. **83**, 1918 (1999).